ATLAS Internal Note
MUON-NO-035
19 January 1994

PART 1

Honeycomb Strip Chambers

for the

ATLAS Muon Spectrometer

NIKHEF-H, Amsterdam, The Netherlands

F. Bakker, G. Bobbink, R. de Boer, G. Brouwer, C. Daum, W. Gotink, H. van der Graaf, H. Groenstege, A. Korporaal, W. Kuilman, G.G.G. Massaro, P. Rewiersma, H. Schuylenburg, S. Sman, H. Tolsma, P. Werneke

University of Amsterdam, The Netherlands

J. Buskens, F.L. Linde

University of Nijmegen, The Netherlands

R. Bergman, C. Brouwer, F. Crijns, J. Dijkema, W. Kittel, A.C. König, C. Pols, E. Visser, T. Wijnen

MSU, Moscow, Russia

S.G. Basiladze, V.A. Kramarenko, A.K. Leflat, V.S. Murzin, S.M. Rouzin, L.N. Smirnova, V.Yu. Zhukov, E.G. Zverev

IHEP, Protvino, Russia

V. Ammosov, V. Gapienko, Yu. Gutnikov, V. Zaetz

Abstract

In this report we describe the use of Honeycomb Strip Chambers for the muon spectrometer of the ATLAS experiment. Principal operation, construction techniques and layout in ATLAS are described. Results from beam tests of prototype chambers and performance simulations are presented.

January 19, 1994

List of Abbreviations:

FB	Forward/Backward (chambers, region)
HHPCB	Hedge Hog Printed Circuit Boards
HSC	Honeycomb Strip Chamber
LEGO block	Mold-injected precision plastic block defining the wire positions
MI	Muon Inner (chamber)
MM	Muon Middle (chamber)
MO	Muon Outer (chamber)
Monolayer	Plane of parallel hexagonal tubes
Multilayer	Stack of monolayers
Octant	$\frac{1}{8}$ section of circle
P1, P2, P3	Prototype 1, 2, 3 (HSC)
RASNIK	Red Alignment System NIKhef
RD5	Research & Development experiment at CERN
Sagitta	Deviation from straight line ($= MM - \frac{1}{2}(MI + MO)$)
Stiffener	Panel, connected to a HSC to limit the HSC sag
Station	Track sampling unit (MI, MM or MO)
TDC	Time to Digit Convertor: electronic unit which notes the moment of threshold crossing of the wire signal.
TRACAL	TRAcing CALorimeter: experimental set-up of iron absorbers and monolayer HSCs
Wire Clip	Small Copper-Tellurium block with a slit which fixes, after crimping, a wire

Coverpage

The foil in the window of the cover of this paper is the material used for the P2 chambers. It is polyesther foil (mylar) with a 1 micron layer of sputtered copper. By means of a printing process which is standard in the packaging industry, a coating is applied where the strips will come. By means of chemical etching the copper between the strips is removed. After this the coating is removed. The width and position of the strips have a precision of 13 μm *(rms).*

Contents

1 The HSC for the ATLAS Muon Spectrometer

To optimise the (stand alone) performance of the muon spectrometer the ATLAS collaboration has decided in favour of the superconducting air core toroid. This magnetic field lay-out allows a precise determination of the sagitta from three precision points (track segments) measured along a muon track, one to the inside (MI), one to the outside (MO), and one in the middle (MM) of the magnetic field region.

The performance of a three-station muon spectrometer will be determined by:

(a) the intrinsic spatial resolution of the MI, MM and MO chambers,

(b) the relative alignment of the stations in a MI-MM-MO tower,

(c) the multiple scattering caused by the material near the middle chamber: magnet coil+services, MM chamber+stiffener and trigger detectors.

In addition to these three error sources the resolution of the muon momentum at the vertex will be affected by the uncertainty in the correction for the energy loss in the calorimeters. This contribution is important for momenta below 30 GeV/c, but in this momentum region the inner detector improves the stand-alone performance of the muon spectrometer considerably.

Multiple scattering is dominated by the magnet (coil and struts) over roughly 50% of the solid angle and by MM chamber + stiffener + trigger over the remaining 50%.

Intrinsic spatial resolution and relative alignment are parameters of the muon chamber system itself and will be discussed in detail in this report.

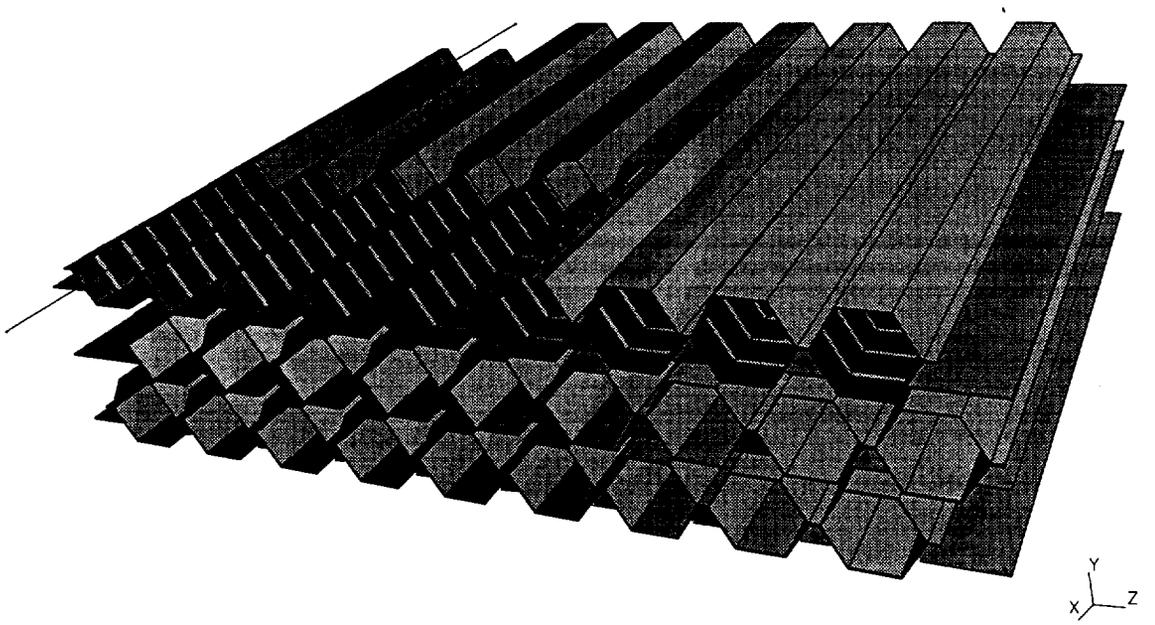

Figure 1: *The Honeycomb Strip Chamber*

Optimal performance of the muon spectrometer requires a balanced approach towards *all* contributions to the muon momentum error. Considering overall accuracy,

design flexibility (number of layers, cell diameter, 2^{nd} coordinate option), amount of material, experimentally demonstrated performance and low cost, we propose the Honeycomb Strip Chamber (HSC, figure 1) as the best solution.

The basic building block of an HSC is the monolayer. It is composed of two folded foils (mylar or aluminium) combined on a template to form a layer of cells of hexagonal cross section. The diameter of the cells can be optimised with respect to background from low energy neutrons and photons and can range from 5 to 40 mm.

Within a monolayer, anode wires are positioned to an accuracy of 18 μm by side combs mounted on both ends. This accuracy can be verified *after* assembly. In addition, the side combs provide an easy connection for high voltage, readout electronics and other services. For chambers longer than 4 m, an additional middle comb is used to support the wires half-way. Optionally, cathode strips can be etched on mylar foils to measure the coordinate *along* the wire direction (2^{nd} coordinate).

Monolayers are stacked to form a multilayer aligned by the precision combs. As is the case for the cell radius, also the number of monolayers in a multilayer is a parameter to be optimised with respect to the particular position in the detector, without changing the technology. Furthermore, multilayers can be split into two halves to improve the angular resolution of the segments of a muon track, and consequently the momentum resolution in regions where the sagitta measurement is spoiled by magnet material.

Depending on the location, a station consists of either one multilayer with aluminium honeycomb stiffener on both sides or a set of two multilayers separated by honeycomb stiffener. By design, the gravitational sag of a station equals the sag of a wire [a], thus keeping a wire everywhere at the center of the hexagonal cell. The weight of a realistic fully assembled MM station of 8.5 m^2 amounts to a total of 220 kg (electronics not included). For the multiple scattering contribution, only 17 kg/m^2, equivalent to $0.06 \times X_0$ has to be considered, since edge materials can be disregarded. Since the contribution of scattering in the MO and MI stations to the momentum resolution is negligible, more material can be applied for these stations to achieve an optimal layout.

In modern construction, ultimate stiffness can be replaced by accurate displacement monitors and correction procedures. The relative position of the two side combs and the middle comb of each multilayer will be ('horizontally') monitored in situ by two CCD/RASNIK alignment systems. Similar systems will be used for the continuous ('projective') monitoring of the relative alignment of the MI, MM, MO stations to an accuracy of 30 μm. As opposed to e.g. the HPDT technology, the integration of these vital alignment systems into the HSC does not introduce additional dead regions.

Three years of R&D and prototyping have resulted in a broad experience with production methods and production tools. The required performance levels have been reached experimentally on large chambers. Further improvement is expected for 1994.

The first HSC prototype, the 8 layer 30×30 cm^2 P1 chamber built in 1990, has been tested extensively over recent years using charged particle beams (X3/L3, RD5) and cosmic rays. Initially the emphasis was on the strip coordinate; later it shifted to the resolution of the wires. The performance (time-distance relation, single cell resolution

[a] The gravitational sag of the longest wires (6.5 m) is 0.85 mm. The combs, on the other hand, are very stiff by construction. The sag of the longest comb (2.2 m) is less than 10 μm.

(wires and strips), efficiency, maximal drift time) was studied for a variety of gases, high voltage settings, magnetic field configurations and incident particle directions. The results were very encouraging [1].

In 1991, a set of 25 monolayers of size 100 × 60 cm^2 has been incorporated into the tracking calorimeter TRACAL of the RD5 experiment, to study hadronic punch-through and effects of muon induced electromagnetic showers [2]. Early 1993, three large (100 × 320 cm^2) 8-layer chambers (called P2) have been built and tested in the muon beam of RD5, together with six CCD-RASNIK alignment systems. Currently, an ATLAS sized 8-layer chamber (P3) with a wire length of 570 cm is being tested at NIKHEF with cosmic muons. This chamber will be moved into the muon beam of RD5 in early 1994.

In these tests, the average single-wire resolution has been proven to reach a level of 100 μm.

The main characteristics of the ATLAS barrel muon spectrometer based on the HSC technology (and already *achieved* performance figures) are summarised in table 1. The number of layers in the MM chamber (16) is twice the number of layers in the MI and MO chambers (8), in view of the relative weight of the MM chamber measurement on the sagitta: $S \equiv MM - \frac{1}{2}(MI + MO)$. The average number of hits is taken to be equal to the number of layers since the geometric inefficiency due to the 1.0 mm gap region between two hexagonal cells ($\approx$ 4% for a 30 mm cell diameter) is easily compensated by the increase in the number of hits for tracks at $\eta > 0.5$.

The increase of the cell diameter from the hitherto tested 11.5 mm to 30.0 mm is expected to improve the average single wire resolution to well below 100 μm due to the reduction of the relative importance of the low-resolution region near the anode wire. This will be verified with the P3 chamber which has a 23.0 mm cell diameter. However, for the calculations presented in this report we keep the average single wire resolution at the proven level of 100 μm.

In the region of solid angle shadowed by the coils and the support structures of the magnet, multiple scattering dominates the uncertainty on the measured sagitta for muon momenta up to about 250 GeV [b]. Outside this shadow region the MM chamber itself (0.061 × X_0 [c]) and the trigger layers around the MM chamber (0.10 × X_0) contribute about equally to the $\Delta p/p$ from multiple scattering.

Neglecting the uncertainty on the energy loss in the calorimeters, the $\Delta p/p$ error budget (HSC chambers & alignment, multiple scattering MM and trigger, respectively) becomes (p in GeV):

$$\frac{\Delta p}{p} = \sqrt{(1.4 \times 10^{-4} \times p^2 + 1.0 + 1.1^2)}\% = \sqrt{(1.4 \times 10^{-4} \times p^2 + 1.5^2)}\%$$

With the above lay-out, the total number of wire read-out channels in the barrel region is 320 000. The cost of the complete barrel and endcap muon spectrometer (excluding the installation itself) is estimated to 18.5 MSFr.

[b] In the present design, the main contribution comes from the stainless steel enclosure of the strut. The stainless steel thickness should be minimised and the separation between these struts and the MM chambers should be maximised.

[c] To be compared with 0.146 × X_0 for the HPDT and 0.035 × X_0 for the JCC

Honeycomb Strip Chamber Muon Spectrometer			
Monolayer			
	Cell diameter	30 mm	
	Gap between cells	1.0 mm	
	Maximum drift time	500 ns	
	<Single wire resolution>	100 μm	
	<Wire position>	18 μm $\oplus$ 18 μm	
Multilayer		MM	MI & MO
	Monolayer distribution	16 or 8 + 8	8 or 4 + 4
	<Number of hits>	16	8
	<Resolution>	31 μm	40 μm
	Amount of material	$0.061 \times X_0$	$0.054 \times X_0$
Tower			
	MI-MM-MO Sagitta	$\sqrt{31^2 + \frac{1}{2} \times 40^2} = 42$ μm	
	Projective alignment	30 μm	
Sagitta	(No multiple scattering)	$\sqrt{30^2 + 42^2} = 52$ μm	

Table 1: *HSC characteristics for the ATLAS barrel muon spectrometer.*

To summarise the main features of the HSC:

Performance: The intrinsic momentum error contribution of the HSC together with the CCD/RASNIK alignment system of $\Delta p/p = 0.012 \times p\%$ (p in GeV) is well matched to the combined multiple scattering contribution of the MM chamber and the trigger chambers of $\Delta p/p = 1.5\%$.

Flexibility: The modularity of the HSC construction (monolayer $\rightarrow$ multilayer) together with the wide acceptable range of the basic cell diameter (occupancy, endcap versus barrel) allows for a flexible i.e. optimal design of the muon spectrometer. In addition, if required in the barrel and/or endcap regions, a precise 2^{nd} coordinate is available without additional construction costs.

Concept: Balance between "accuracy by construction" (the wire combs) and "accuracy by monitoring" (along the wires within a multilayer and along the edges of the projective towers). This is a cost effective solution, since heavy chambers and/or complicated support structures are avoided. In addition it permits a continuous verification of the inter/intra chamber alignment.

Installation: The actual installation of any muon spectrometer will be a tour de force and requires a major engineering effort. The 17 kg/m^2 weight of the HSC and the monitoring instead of stiffening approach towards deformations (gravity, temperature etc.) clearly facilitates the installation process.

Experience: Three years of R&D have led to proven production tools and methods. Large chambers have been tested and the required performance levels have been demonstrated. Recently the vital CCD/RASNIK alignment system (an improved version of the RASNIK system as operated by the L3 experiment) has been integrated with three large HCS chambers.

Cost: The cost is estimated to be 18.5 MSFr.

2 The Honeycomb Strip Chamber

2.1 The chamber principle

The chamber is constructed from folded conductive foils shown in figure 2. Two of these foils are combined to form a layer of parallel hexagonal tubes.

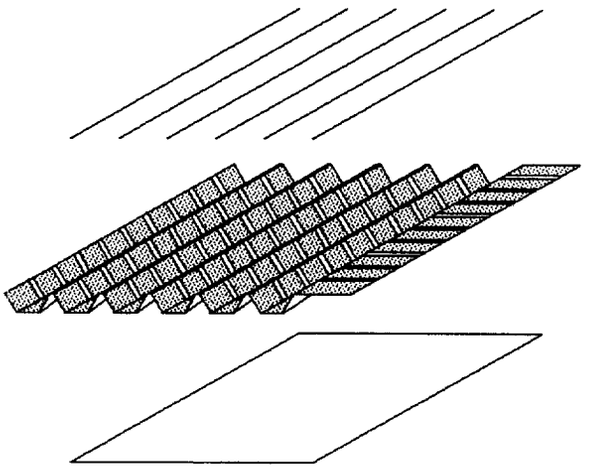

Figure 2: *Schematic reproduction of the assembly of a monolayer.*

A stack of these layers forms a stiff and light block of honeycomb as shown in figure 3.

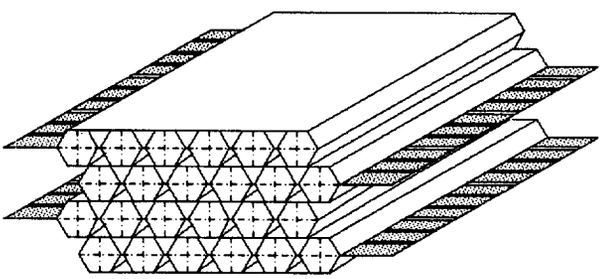

Figure 3: *Stack of monolayers forming a rigid honeycomb structure.*

In the centre of each hexagonal cell a wire is strung. By measuring the drift time, the distance between a muon track and a wire can be determined. Combining the drift distance measurements from all the layers results in a high-precision measurement of the muon track coordinate perpendicular to the wires.

The aluminium foil of selected chamber layers can be replaced by mylar foil with copper strips, oriented perpendicular to the wires. The strips then take the form of hexagonal rings around the wire as shown in figure 4. The charge distribution over these rings allows a determination of the 2^{nd} coordinate of a track.

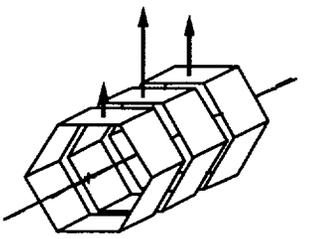

Figure 4: *Three hexagonal rings, forming the basic elements of the HSC with strip readout to determine the coordinate along the wire direction.*

2.2 The construction of the chambers

2.2.1 The construction of monolayers

A basic tool for the construction of monolayers is the template. By means of a special reel (figure 5), the aluminium foil is folded and put in position on the template. As

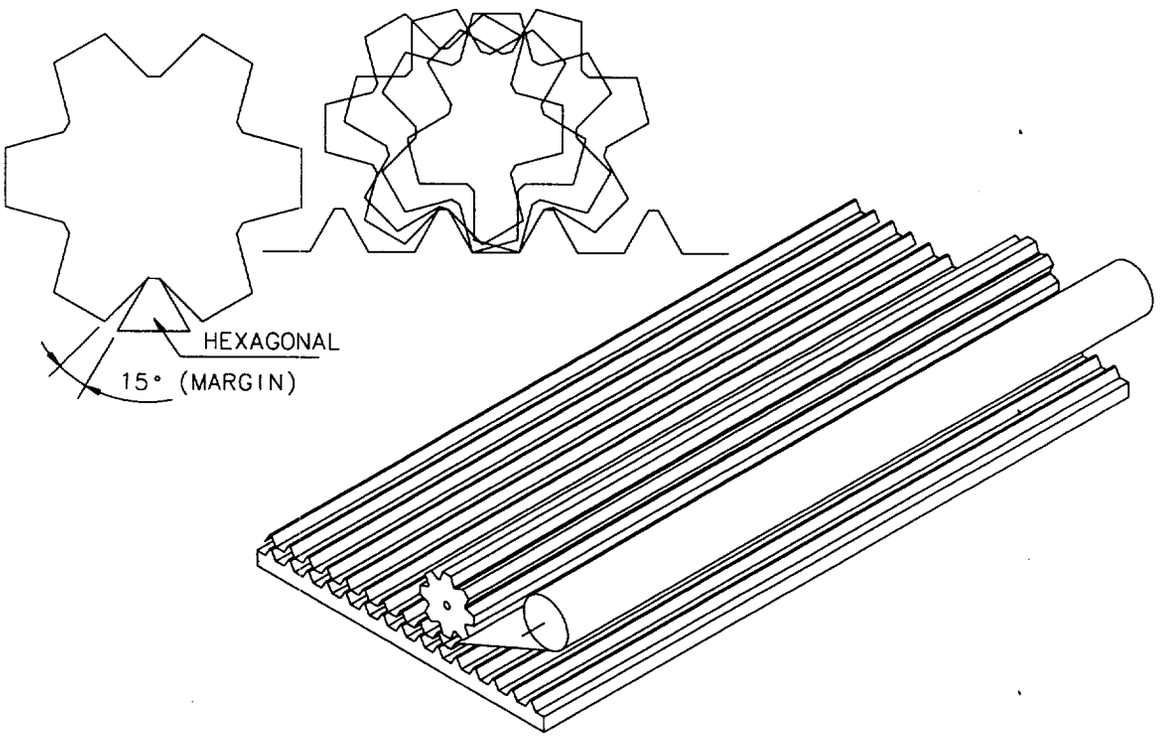

Figure 5: *Reel and template used to fold aluminium foils.*

opposed to the stringent requirements on the position of the wires, the required precision of the folds (straightness, cell radius and shape) is of the order of 300 μm and can easily be met with this technique.

For the prototypes constructed so far (with wire *and* strip readout), we used another technique to fold the mylar foils with etched cathode strips. This folding machine is

shown in figure 34. The assembly of monolayers is identical for mylar and aluminium foils.

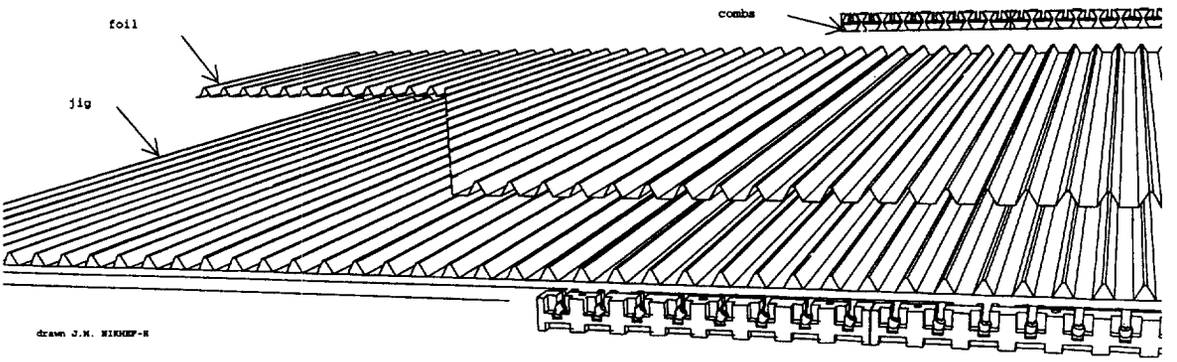

Figure 6: *Schematic assembly of monolayer: foil-template and end-combs are shown.*

The monolayer construction process is illustrated in figure 6. By applying a vacuum between the template and the foil, the foil is pressed tightly in position. For monolayers with a wire length greater than the practical foil width, foils can be connected by overlapping foil strips. When all foils are in position, plastic mould-injected edge blocks are glued at the cell ends. The blocks have reference holes which correspond with precision pins in the template. This block is shown in figure 7. Two adjacent

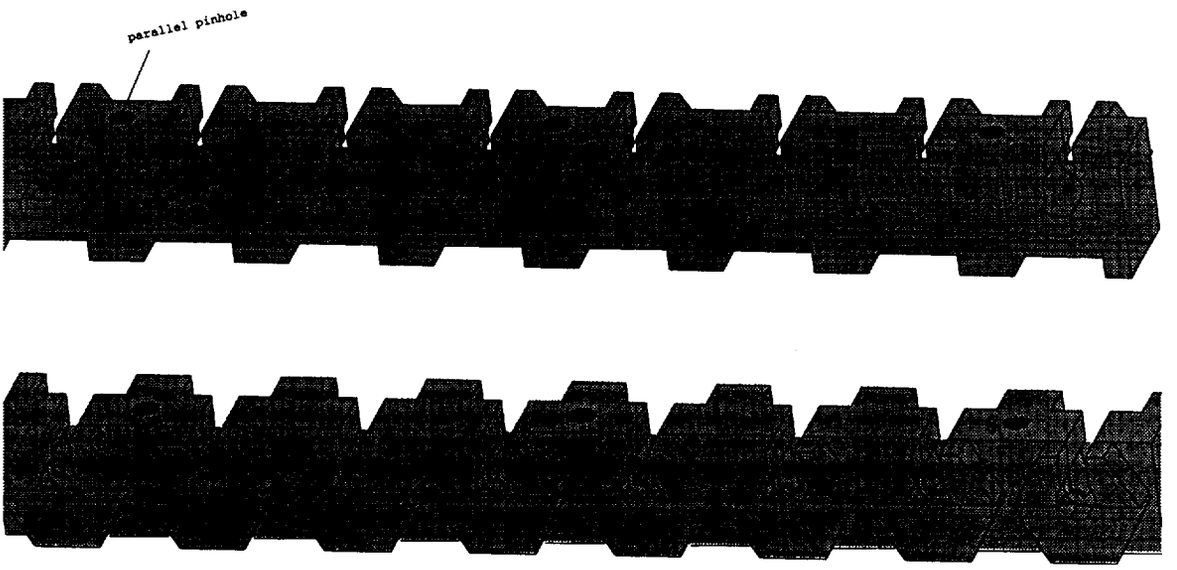

Figure 7: *The plastic mould-injected edge blocks. Top: outer side (the Cu/Te blocks with the slits for wire fixation are not in place). Bottom: inner side; the hexagonal shape of the individual cell is clearly visible.*

blocks are separated by a narrow gap, filled with glue when the blocks are in position on the template. As a result, two continuous plastic edge strips run over the entire

width of the chamber. If the total wire-length of the chamber exceeds 4 meter, an additional wire support is needed. For this we use similar strips.

In the next step the wires are mounted: they are fixed by crimping the slitted Cu/Te blocks [3] which are glued in the plastic edge blocks. The wire position is defined by the slits in the edge blocks. The top foil is prepared in a second template and lowered onto the bottom foil. The two foils are joined by using glue, spot welding or ultrasonic welding. Then the top template is removed and a flat foil is added to complete the monolayer. An auxiliary frame is used to remove the monolayer from the bottom template, without loosing its shape. The monolayer can be inspected (the wires are visible in the plastic blocks and their positions can be verified), stored or combined with other monolayers into a multilayer.

2.2.2 Multilayer assembly

The multilayers are assembled on a flat table. The table is constructed from straight rulers which support the plastic strips (end-combs) holding the wires. The first monolayer is fixed on the assembly table using the screw holes in the plastic edge strips and the side profiles. Then the auxiliary frame is removed. The monolayer still has its original shape, defined by the monolayer template. In the next step, the second monolayer is glued on top of the first monolayer. The relative position of the monolayers is fixed by means of dowel pins inserted into reference holes in the plastic edge strip. The auxiliary frame is removed before the glue has cured: the plastic edge strips of the second monolayer are uniformly pressed onto the first one. This guarantees the positioning of the wires in the plane perpendicular to the chambers (Y direction). The next monolayers are assembled in an identical way. The stacks of edge strips and the middle support strips form the precision wire edge and middle-combs.

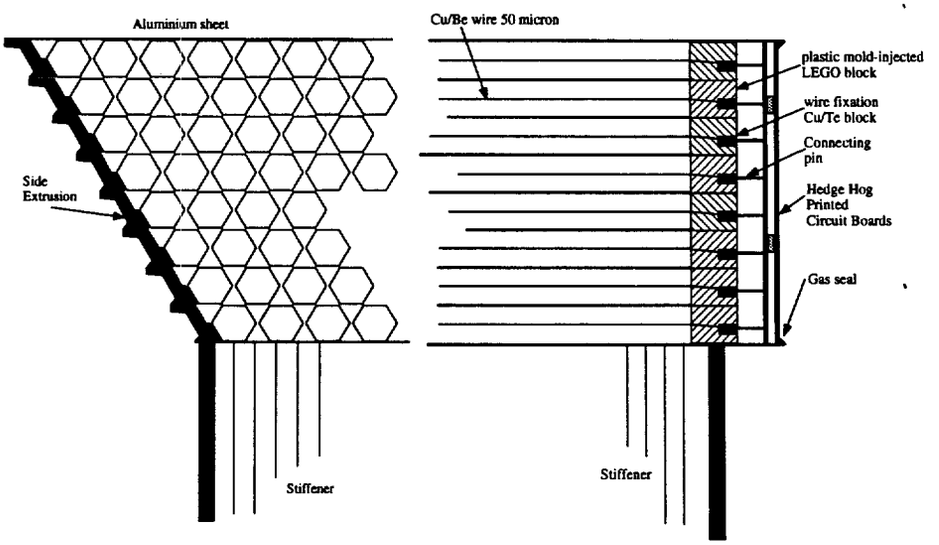

Figure 8: *Cross-sections of a multilayer: a) perpendicular to the wires; b) perpendicular to the end-combs.*

Figure 8 shows cross-sections of the multilayer perpendicular to the wires and the

end-combs, respectively. The Hedge Hog Printed Circuit Boards (HHPCBs) shown in figure 8 have a three-fold function:

- wire signal feedthrough;
- HV distribution;
- gas seal.

The inner PCB is equipped with pins which stick into the Cu/Te blocks. On one side of the wire the print is equipped with decoupling capacitors (1 nF, 3500 V) and on the other side a resistor of 1 $M\Omega$ is mounted to put HV on each wire. The wire amplifiers may be mounted on the 'readout' HHPCB. A second PCB is mounted via connectors on the HHPCB. The gas seal is applied at the edge of this second PCB. As a result the inner HHPCBs, which carry HV, are situated in the dry chamber gas, thus avoiding surface moisture currents. The outer PCB may carry the discriminators, TDC and DACQ ASICs.

As an alternative the individual monolayers could be equipped with a strip-shaped PCB integrated with the monolayer edge-comb. The advantage would be that a monolayer would be a complete gas-tight chamber which could be tested before the assembly of a multilayer.

2.2.3 Station assembly

The stations consist of either :

- one multilayer with aluminium honeycomb stiffener on both sides (figure 9),
- two multilayers with honeycomb stiffener in between (figure 10).

The thickness of the single stiffener for the second type is between 15 cm and 30 cm; depending on the chamber size, number of layers and demands on chamber weight.

The stiffeners consist of aluminium honeycomb covered on both sides with thin aluminium sheets (0.5 mm). They are connected with the multilayers by aluminium profiles of a precise width mounted on the chamber edges (at the end-combs) and the additional wire supports (the middle-comb).

The chambers are designed (via the thickness of the stiffener) to have a sag equal to the sag of the wires. Consequently, the wires are in the centre of the hexagonal cells over the entire wire length. In order to obtain the right curvature, the support feet have to be located near the edge of the chambers under the two end-combs. It may be attractive to use the 3 foot suspension shown in figures 9 and 10. This is possible due to the stiffness of the end-combs (less than 10 μm sag over a length of 2.2 m).

2.3 Mechanical parameters of an assembled station

All components (aluminium foil, mold injected plastic blocks [d]) have thermal expansion coefficients very close to the thermal expansion coefficient of the aluminium template.

[d] The thermal expansion coefficient of the mold injected plastic blocks is controlled via doping (glass) during the production process.

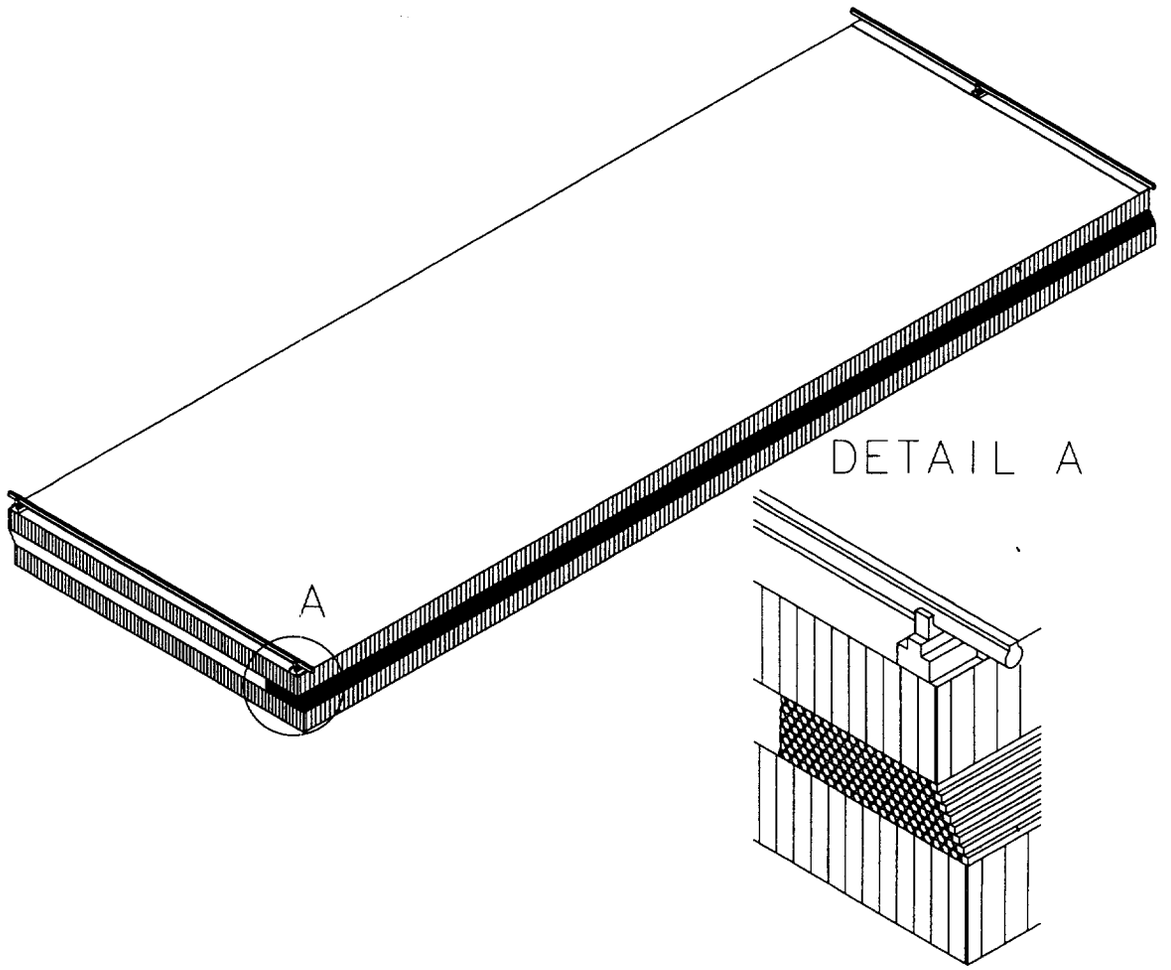

Figure 9: *Station: HSC multilayer with stiffener on both sides.*

Therefore, the ambient temperature does *not* need to be constant during the assembly of a monolayer/multilayer. A completed station can be regarded as a box with the thermal expansion coefficient of aluminium (23×10^{-6}/K).

For the discussion of the crucial uncertainty of the wire positions within a station, we take a large MO chamber as an example. All tolerances given are r.m.s. values. The coordinate system is defined with X along the wires, Y perpendicular to the chamber plane and Z along the beam direction.

1. Mold injected plastic blocks (figure 7): The outer dimensions (30 mm cell diameter) are: $X = 10$ mm, $Y = 30$ mm and $Z = 250$ mm. The tolerances on the relative positions of the wire slits and the reference holes are: $\Delta Y = \Delta Z = 10$ μm.

2. Aluminium template for monolayer assembly: The outer dimensions are: $X = 6500$ mm, $Y = 25$ mm (thickness) and $Z = 2200$ mm. The tolerances (overall, excluding temperature scaling effects): $\Delta X = 0.5$ mm, $\Delta Y = 1.0$ mm and $\Delta Z = 100$ μm. The important tolerances on the reference holes used to position the

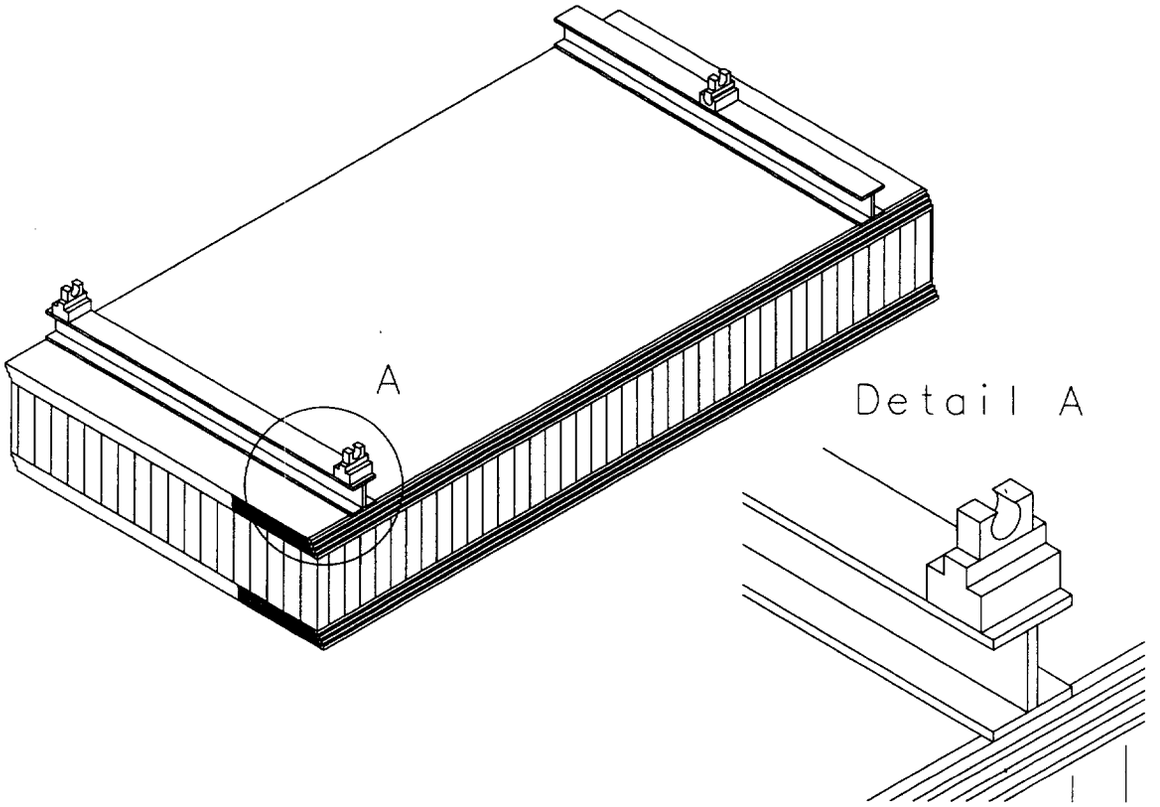

Figure 10: *Station: two HSC multilayer with stiffeners in between.*

mold injected plastic blocks are: $\Delta X = 50$ μm, $\Delta Y = 20$ μm and $\Delta Z = 10$ μm. The X and Z axes are perpendicular to better than 0.1 mrad.

3. Flat table for multilayer assembly: The flatness of the table is better than 0.1 mm over the full surface. Since the wire positions are defined by the end-combs and, if the wire length exceeds 4 meters, the middle-comb, the combs are supported by accurate straight rulers: $\Delta Y = 10$ μm. These straight rulers set the precision; *not* the overall flatness of the table.

As a result, the wire-to-wire precision and wire-to-reference hole precision within a monolayer equals 18 μm (in Z), apart from an overall scaling error. All the monolayers within a multilayer come from the same template. The monolayers are therefore identical to within 18 μm.

The relative positioning of the monolayers is obtained by inserting precision pins into the corresponding reference holes of the mold injected plastic blocks (see figure 7). If n pins are applied per end-comb (or middle-comb), the additional errors ΔX and ΔZ in wire-to-wire positions for different monolayers equal $18/\sqrt{n}$ μm. For m monolayers the error is $18 \times \sqrt{m/n}$ μm. For an 8-layer chamber with 8 pins per comb the additional error equals therefore 18 microns.

The error in the wire-to-reference hole position (anywhere in the chamber) of an 8-layer chamber with 8 pins per end-comb equals $\sqrt{18^2 + 18^2} = 25$ μm.

The edge combs and middle-combs are very stiff: the sag is less than 10 μm for a 2.2 m long comb. The additional uncertainty in the Y position of the wires at the comb due to gravitational sag of the comb itself is therefore negligible. Between the combs the wires (and the chambers) will sag: e.g. a 6.5 m long wire will sag 0.85 mm. This sag (and other deformations) is monitored by two CCD/RASNIK alignment systems. The lenses of these systems are mounted on the middle-comb (if any), the CCD cameras and the masks are mounted on the two end-combs. The positioning of the components of the CCD/RASNIK system with respect to the wires contributes 15 μm to the uncertainty in the wire location, both in Y and Z. The uncertainty in the wire tension (needed for the calculation of gravitational sag) contributes another 10 μm. (This is the maximum value, valid in the middle between two wire supports.) Combined, this gives an additional $\sqrt{15^2 + 10^2} = 18$ μm uncertainty in the Y position of the wires *between* the combs. Those are the results for the extreme case of horizontally mounted chambers. For vertically mounted chambers the gravitational sag effects are negligible.

In section 5 the alignment issues (within a single multilayer and between the three multilayers used for a sagitta measurement) are discussed in more detail.

3 HSC Testbeam Results

3.1 Produced prototypes

In this section a brief overview is given of the development of Honeycomb Strip Chambers since the start of the project. Four different chamber types have been designed and constructed at NIKHEF. The main characteristics of these detectors are given in table 2.

Characteristics	P1	TRACAL	P2	P3
year	1990	1991	1992/93	1993
# constructed	1	25	3	1
# wires/layer	24	48	255	8
# strips/layer	54	192	192	–
# layers/chamber	8	1	8	8
outer cell radius (mm)	5.77	5.77	5.77	11.54
wire length (m)	0.3	1.0	1.0	5.7
wire diameter (μm)	20/30	30	30	50
wire pitch (mm)	12.7	12.7	12.7	25.0
strip length (m)	0.3	0.6	3.2	–
strip pitch (mm)	5.08	5.08	5.08	–
plane pitch (mm)	10.7	–	10.64	20.0
foil material	Kapton	Melinex	Mylar	Mylar
copper thickness (μm)	17	0.3	0.8	0.8

Table 2: *Characteristics of the HSC prototypes.*

The Tracking Calorimeter (TRACAL) [2] detector in the RD5 experiment [4] consists of stainless steel absorbers interleaved with 25 single-layer HSCs as active medium. Normally, a honeycomb structure has an intrinsic mechanical stiffness. In the single-layer geometry used in TRACAL however, this stiffness is provided by a brass frame and a rigid aluminium cover (thickness 2 mm). The main purpose of the RD5 experiment is to measure the probability for and the angular momentum distributions of punchthrough particles. TRACAL has proven to be a useful detector for this purpose. Moreover, the strip read out of the HSC's has provided a tool to recognise muon induced electromagnetic showers (see [5] and Appendix C).

The prototypes P1, P2 and P3 are all multi-layer chambers. They consist of 8 active layers and sometimes 2 additional layers for stiffness and shielding purposes. The hexagonal shape of the foil of the P1 detector was obtained by thermal deformation. All other foils were folded on a specially designed folding machine (see Appendix A and figure 34).

Results from the analysis of test beam experiments performed with P1 and P2 are presented in this report.

The construction of the last prototype P3 was finished in December 1993. The chamber is now in a cosmic ray setup at NIKHEF. Preliminary results obtained from these tests are presented in section 3.5.1. Furthermore, an elaborate test of the P3 chamber - inside the 3 T EHS magnet at the RD5 experiment - is foreseen in April and June 1994.

3.2 Strip readout

A comprehensive report on the front-end electronics, data acquisition and performance of the strips is given in reference [1]. Further details are given in Appendix A.

3.3 Wire readout

In 1990 the P1 chamber was tested at the L3 test site at CERN [1]. In these tests the gas mixture and high voltage settings were optimised for a good strip performance.

The drift cell performance of P1 was tested in 1992 in a cosmic ray setup at NIKHEF, where the number of read-out channels was limited to 4 wires/layer (wire diameter 20 μm). Results were obtained for different gas mixtures of Ar and CO_2. The analysis of these results also invoked the so-called autocalibration algorithm to be discussed in detail in the next section (section 3.3.1).

In autumn 1992 the P1 chamber was installed in the RD5 experiment where its behaviour was studied in muon beam conditions. More extensive tests were performed in September 1993, when it was positioned inside the 3 T EHS magnet. All wires (30 μm diameter) were connected to the data acquisition, whereas the cathode strips were attached to ground.

Simultaneously to this last P1 test, the three P2 chambers were installed and tested in a projective setup in the RD5 experiment. Data from both the wires and the strips were recorded. Moreover, six CCD/RASNIK systems were installed on the three P2 chambers. These systems took data over a continuous period of 2 weeks.

3.3.1 Autocalibration

One of the important issues to obtain a good spatial resolution is to find the correct relation between the measured drift time (t) and the drift distance (r). This $r-t$ relation depends on the gas (mixture, pressure and temperature), HV, cell geometry, local magnetic field and the angle of incident particle (θ), due to the hexagonal shape of the drift cell (see section 3.3.3).

To calculate the $r-t$ relation to the needed accuracy is a complicated procedure if one takes all of the above mentioned items into account. A more direct and reliable method to obtain this relation is to deduce it from the muon track data themselves. This procedure is called "autocalibration".

An experimental $r-t$ curve [e] is used to reconstruct the muon tracks in first order

[e] To initialise the autocalibration the experimental $r-t$ relation can be an arbitrary function, such as $r = \text{Const} \times \sqrt{t}$. A better approximation can be obtained by the normalisation of the time spectrum $(0 - t_{\max})$ over the range of drift distances $(0 - r_{\max}$, with $r_{\max}$ equal to the cell radius), assuming a uniform hit distribution over the cell.

(figure 11a). Residuals are calculated in slices of drift distance (r) for a data sample of typically 5000 events. The shift of the mean value in the residuals of each slice gives the correction to be applied to the initial $r - t$ relation (figure 11b-top). Since there are no external track defining points, the trackfit only depends on the erroneous input $r - t$ relation. The final $r - t$ relation can, therefore, be found by repeating the procedure several times. Initial and final (15 iterations) $r - t$ relation are shown

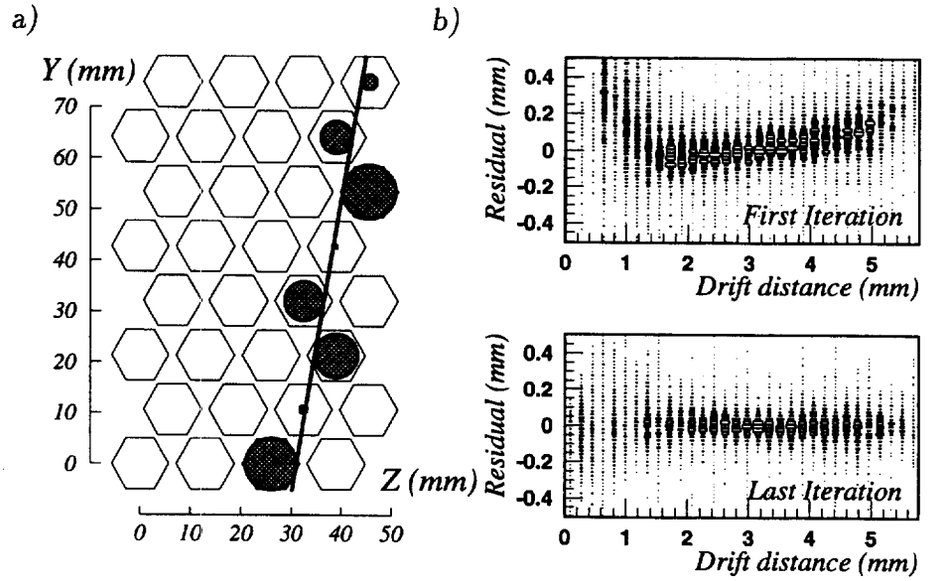

Figure 11: *a) Example of a track measured with the HSC; b) Residuals in slices of the position in the cell before (top) and after (bottom) autocalibration.*

in figure 12a for a data sample taken with cosmics. The initial curve has the general equation $r = \text{Const} \times \sqrt{t}$. The corresponding residuals for the 1^{st} and 15^{th} iteration are shown in figure 11b.

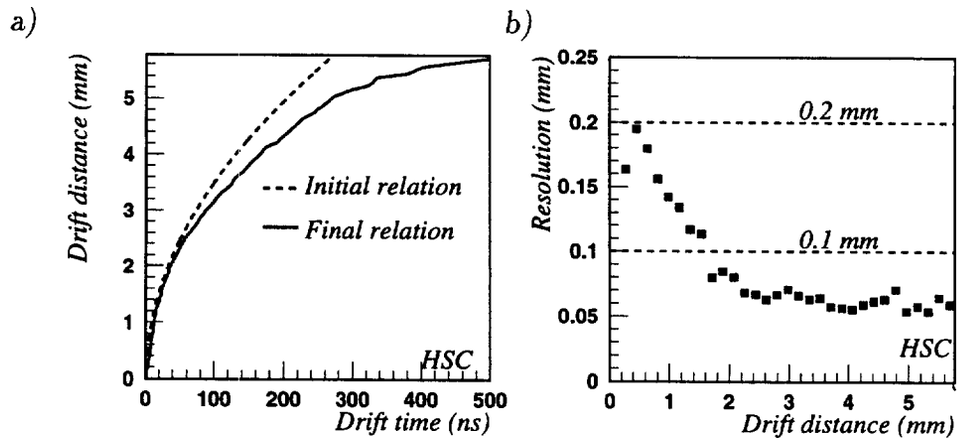

Figure 12: *a) Initial and final $r - t$ relation. b) Spatial resolution as function of the drift distance ($r_{max} = 5.77$ mm).*

Clearly, the spatial resolution improves whenever a more realistic $r - t$ relation is

used. The gaussian width of the residuals is used (for every slice of r from fig. 11b) to deduce the spatial resolution as a function of the drift distance (see figure 12b). The increase of the width close to the wire ($r < 1.5$ mm) is caused by primary ionisation statistics.

Averaged over the entire drift cell the resolution is approximately 100 μm. This number will improve for larger cell radii due to the reduced effect of the region near the wire. However, for very large cell radii (> 50 mm) the resolution will become worse again due to diffusion ($\propto \sqrt{r}$).

3.3.2 Measurements in a magnetic field

To investigate the performance of HSCs inside a magnetic field, the P1 chamber was positioned in the 3 T EHS magnet. The magnetic field orientation was perpendicular to the incident particles and parallel to the wires (for $\phi = 0^o$). Measurements were done with several values of the following parameters:

- Muon momentum (100, 200 and 300 GeV),
- Magnetic field strength (0, 0.5, 1.0, 1.5, 2.0 and 3.0 T),
- Angle θ (0^o, 5^o, 15^o, 30^o and 45^o),
- Angle ϕ (0^o, 5^o, 10^o, 15^o and 25^o),
- High voltage (1600 V - 2600 V),
- Gas mixture $Ar/CO_2/CF_4$ (fractions: 80/20/0, 50/50/0, 68/17/15 and 56/14/30).

A detailed analysis is still in progress, but the preliminary results - to be presented below - show excellent behaviour of the multi-layer HSC inside a magnetic field, even at B=3 T. The spatial resolution is maintained despite the change in the $r-t$ relation due to variation of the magnetic field strength, causing a variation in the path length of the drifting electrons.

The average magnetic field strength in the barrel region of ATLAS will be 0.5 T, but it can be as high as 1.5 T close to the coils. Therefore, the HSCs will be well suited for the magnetic field of ATLAS.

During the P1 test, twelve adjacent wires were read out in each layer. The 96 signals were fed into a hybrid preamplifier [6], digitised by a discriminator [7] and transported along twisted pair cables to the TDC's[f].

The initial $r-t$ relations are shown in figure 13a for B = 0, 1.5 and 3.0 T (Ar/CO_2 50/50). The increase of the drift time with increasing magnetic field strength is clearly visible.

The resolution is calculated as a function of the drift distance after autocalibration. For B $\neq$ 0 T, the 'drift distance', defined as the shortest distance between the track of the incident particle and the anode wire, is no longer equal to the actual path length of the drifting electrons.

[f] LeCroy, CAMAC Time-to-Digital-Converter 2277

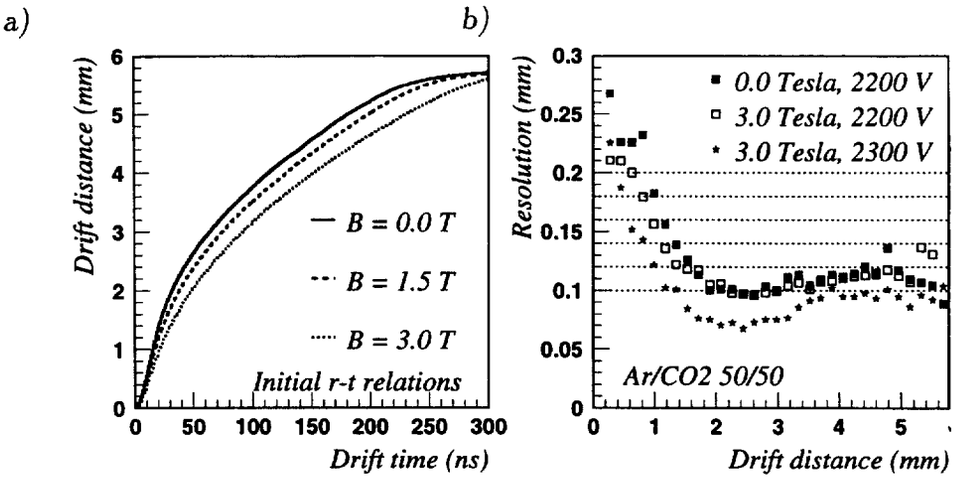

Figure 13: *a) Initial $r-t$ relations for three magnetic field strengths; b) The spatial resolution (as a function of r) for different gas gains and magnetic field strengths.*

Several measurements were performed with different high voltage and angle of incidence θ for each magnetic field setting. The angle θ has no influence on the spatial resolution per layer, but the resolution changes dramatically with the high voltage due to the difference in the gas gain.

Resolution curves for B = 0 T and 3 T are plotted in figure 13b, the latter are given for HV = 2200 V and 2300 V. The difference in resolution for the different HV values can be observed clearly. Data for other magnetic field settings are not available at HV = 2300 V, due to insufficient running time at the SPS. Comparing at HV = 2200 V, the performance of the detector is unaffected, despite the changing $r-t$ relation.

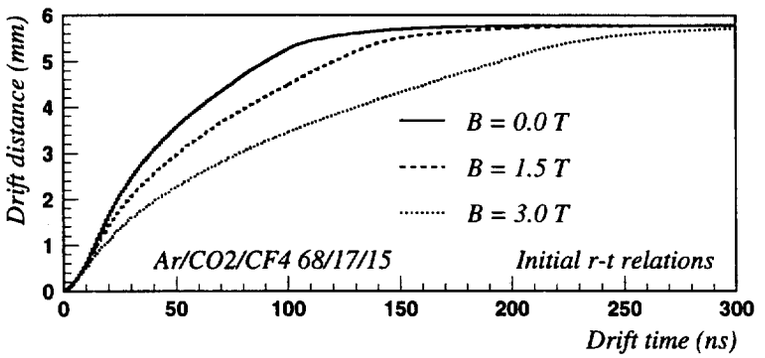

Figure 14: *Initial $r-t$ relations for different magnetic field strengths for an $Ar/CO_2/CF_4$ mixture.*

Preliminary analysis of the $Ar/CO_2/CF_4$ 68/17/15 data results in the $r-t$ relations for B = 0, 1.5 and 3.0 T, shown in figure 14. The increase of the drift time with increasing field strength in this gas mixture is larger than for the Ar/CO_2 50/50 mixture. This larger drift time can be understood from the larger Lorentz angle of this mixture. An advantage is the short drift time in the regions of low magnetic field. The gas

mixture can be optimised according to the requirements for the ATLAS spectrometer. The composition of the gas will be discussed in section 3.3.4.

3.3.3 Angle of incidence θ

There is no θ dependence to be expected in the drift characteristics of a round drift tube. For a hexagonal tube, however, there is a non-uniformity of the drift field in θ with a periodicity of $2\pi/6$. The hexagonal geometry can be taken into account by applying θ dependent higher order corrections to the field in a round tube. From theoretical studies one can conclude that the $r-t$ relations only differ significantly in the outermost regions of the cell [8].

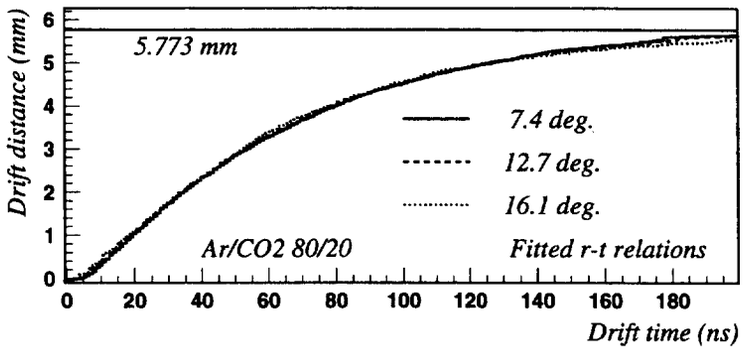

Figure 15: *Final $r-t$ relations for three different angles of incidence θ. The data are taken with a P2 in the RD5 experiment.*

In figure 15, the final $r-t$ relations are shown for data taken with one of the P2 chambers. The chambers are tested in the muon beam of the RD5-experiment. Data are taken at $\theta = 7.4^o$, 12.7^o and 16.1^o, representing different regions along the beam direction in the ATLAS barrel. The curves in figure 15 coincide for most of the drift range. The curves start to differ from each other, as expected, only close to the cell border. The testbeam experiments show that the θ dependence is very small indeed and can (if desired) be corrected using the data.

3.3.4 Gas studies

Tests were done with different Ar/CO_2 and $Ar/CO_2/CF_4$ mixings. Most of the test were done with Ar/CO_2 50/50 which is a relatively slow gas, but provides a good spatial resolution. Adding argon up to a ratio of Ar/CO_2 80/20 makes the gas faster, while keeping it cheap and non-flammable.

Adding some CF_4 to the Ar/CO_2 80/20 mixture makes the gas even faster, but also more expensive. The use of CF_4 may also be restricted in the future for environmental reasons. In figure 16a the $r-t$ relations are shown for the Ar/CO_2 mixings discussed above. The measurements were done in 1992 in a cosmic ray setup at NIKHEF. The corresponding resolution curves (after autocalibration) are shown in figure 16b. The superiority of the resolution for the slower gas cannot be explained completely by the

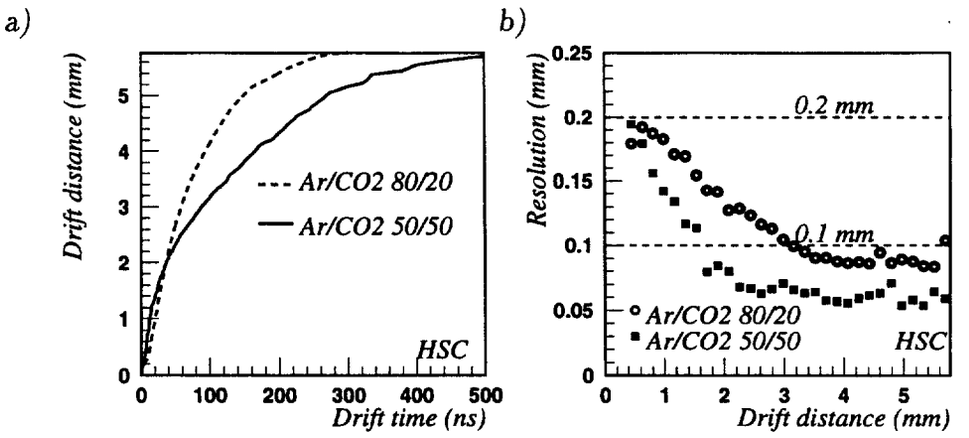

Figure 16: a) *The $r-t$ relations for two Ar/CO_2 mixtures; b) Measured resolutions for the same gasmixtures.*

decreased sensitivity on the error in the measured drift time. Most likely, the gas gain was higher for the data taken with the 50/50 mixture.

The θ acceptance of the setup was $\pm$ 30°. The autocalibration on the data was applied without any cut on θ. The curves in figure 16 show again that neglecting the θ dependence in the drift field introduces only a small error.

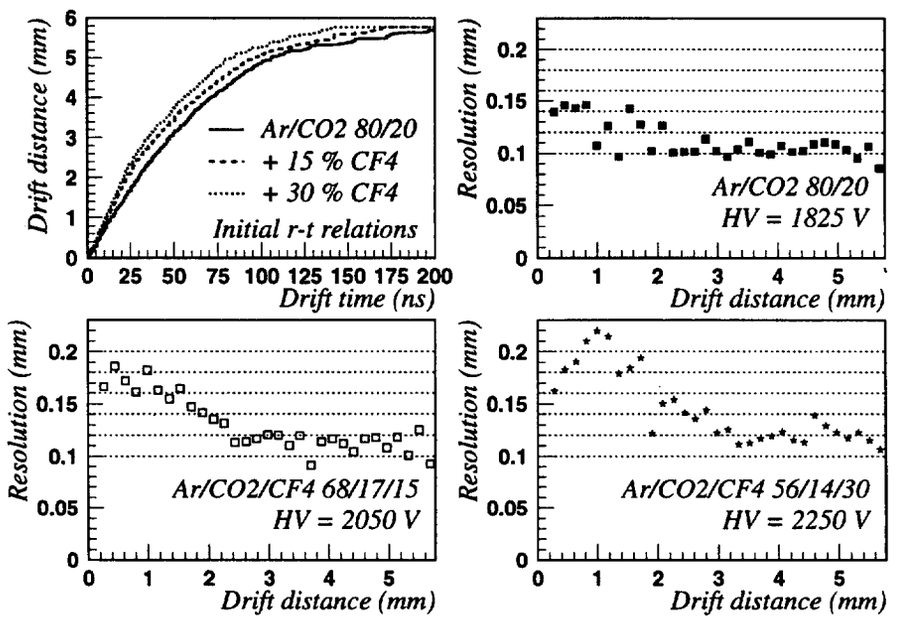

Figure 17: *$r-t$ relations measured for three different mixtures of $Ar/CO_2/CF_4$ and the corresponding resolution curves.*

The $r-t$ curves and resolution plots corresponding to data taken with CF_4 added to an Ar/CO_2 80/20 mixture are shown in figure 17.

3.4 Sagitta measurement with three P2 chambers

Three P2 chambers were installed in the RD5 experiment. The most upstream chamber was positioned 30 cm behind 1.20 m of iron to generate electromagnetic showers. From each layer, 16 wires and a variable number of strips were read out by a VME Transputer system with a transputer link to the RD5 DAQ. The setup of the experiment is shown in figure 18.

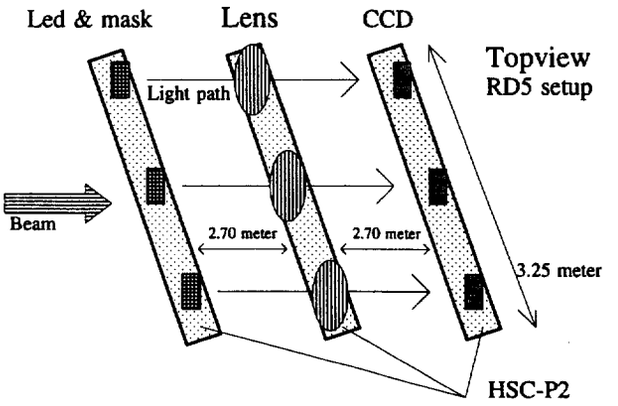

Figure 18: *Setup of the RD5-P2 experiment*

The analysis of the data is still in progress, but preliminary results give less than 85 μm for the spatial resolution of the strips. The spatial resolution obtained with the wires depends on the type of electronics used. Under experimental conditions similar to the P1 tests, the results are equal to that of the small prototype. In figure 19a the

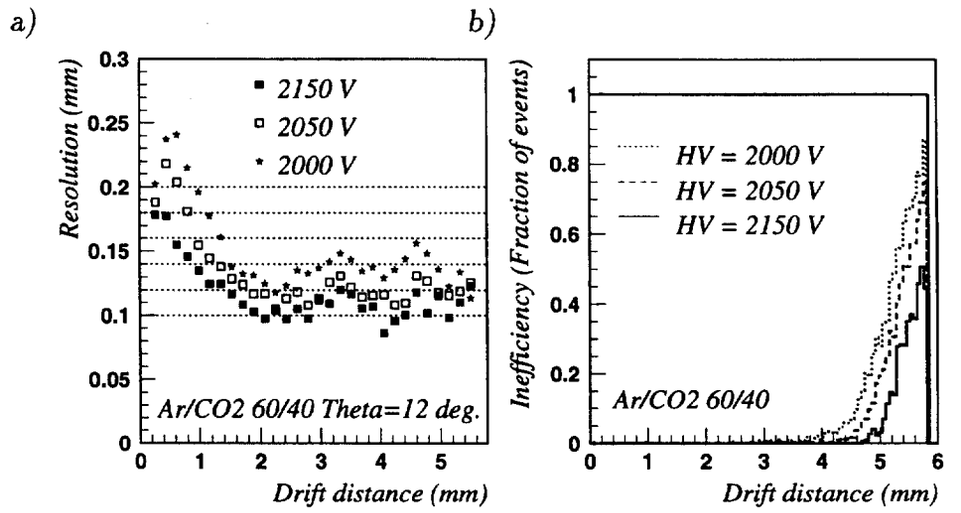

Figure 19: *a) Resolution curves of the P2 for three high voltages; b) Corresponding inefficiency curves. The outer radius of the cell is 5.77 mm.*

spatial resolution curves are shown for several high voltages. Unfortunately, the high voltage could only be as high as 2150 V because of surface currents on the printed

circuit boards. This limits the average wire resolution to $100 - 150\ \mu$m. (This current was due to moisture on printed circuit boards. This problem is solved for the P3 chamber, where an additional cover is used, also for service reasons.

The inefficiency of a single HSC cell is shown in figure 19b for three HV settings as a function of the drift distance. The efficiency drops in the outer region of the cell because of the decreasing gas gap.

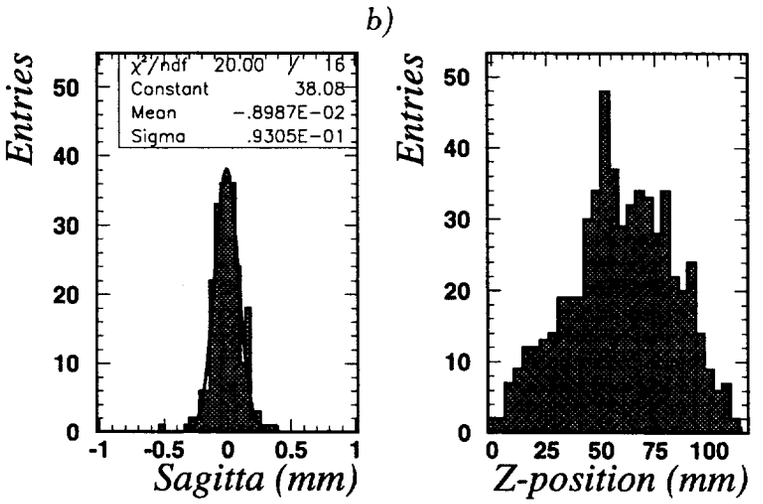

Figure 20: *a) Sagitta measured with the P2 chambers in absence of a magnetic field; b) Beam profile of the RD5 muon beam (200 GeV) in the first chamber.*

Combining the data of the 3 individual chambers, a sagitta S can be measured ($S = Z_2 - \frac{1}{2}(Z_1 + Z_3)$ from the $Z_{1,2,3}$ coordinates measured with the wires). The preliminary result on the measured error in S is 93 μm (see figure 20a). To reduce this error, the relative alignment of the three chambers has to be better understood.

On the chambers, 6 CCD/RASNIK alignment systems were installed (see [9] and Appendix D). Unlike the situation in ATLAS, the relative position of the CCD/-RASNIK components with respect to the wires was unknown. Therefore these CCD/-RASNIK systems can only be used to correlate changes in the measured sagitta with changes in the chamber positions. To study this, the middle chamber was moved along X,Y and Z to compare the introduced shift in the sagitta with the sagitta measured from the muon tracks. This analysis is still in progress.

3.5 The P3 chamber

P3 is an eight-layer Honeycomb Chamber with dimensions as summarised in table 2. The outer cell radius is 11.6 mm, approximately the dimension of the cells in the ATLAS chambers. Figure 21 shows the cross section of the chamber. The length of the wires (perpendicular to the plane) is 5.7 meter. The cathode plane consists of folded Mylar foil with copper strips. The strips are not read out, but put on ground potential. An additional shielding foil between the monolayers prevents cross talk. The 50 μm wires are clamped in Cu/Te blocks which were mounted in the LEGO blocks.

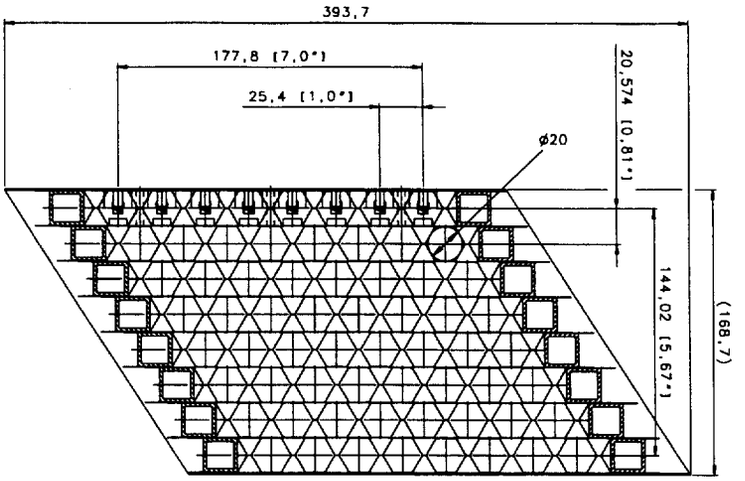

Figure 21: *Cross section of the P3 detector*

The stack of eight LEGO blocks forms the end-comb. The wires were supported by an additional comb in the middle of the chamber.

3.5.1 Cosmic ray results

Cosmic ray tests are performed over a period of three weeks. P3 is operated with a gas mixture of Ar/CO_2 50/50 at a high voltage of 3000 V, the limit before entering the streamer mode.

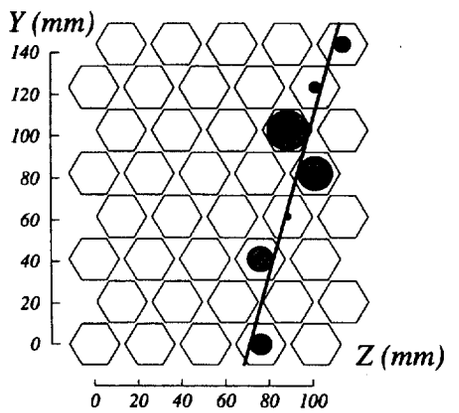

Figure 22: *Typical event measured with P3.*

Figure 22 shows a typical event. Five wires are read out per plane. Two scintillators limit the coordinate along the wire to a range of 15 cm. The principle of autocalibration is applied as on the P1/P2 data and the residuals areresiduals are calculated as before. Figure 23a shows the raw time spectrum with the maximum drift time over 1000 ns, typical for this slow gas. Figure 23b shows the $r-t$ relation for the first approximation and after 15 iterations of autocalibration. These curves were calculated with a loose cut on the angular acceptance ($|\theta| < 0.5$ rad). The θ-dependence of the space-time relation

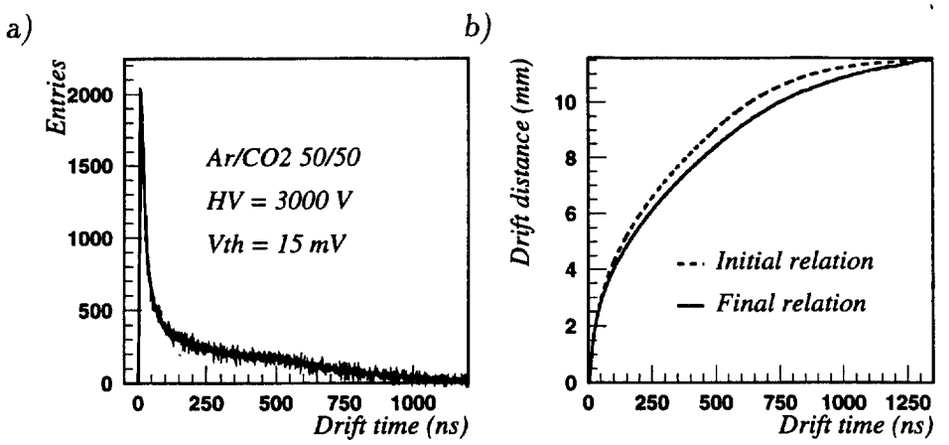

Figure 23: *a) Drift time spectrum; b) Drift time vs. drift distance relations before and after autocalibration.*

becomes more important for a large cell. This effect can be visualised by calculating the resolution without any cut on θ and by applying a cut. The resulting resolution plots are given in figure 24. The improvement achieved with the cut is evident. The rise of the resolution for large r is not yet understood.

3.5.2 Plans with P3

The following topics will be studied in the near future:

- Verification of mechanical stiffness, finite element calculations.
- Variation of resolution as a function of the position along the wire,
- Variation of the Z-position of the wires along the wire,
- The Y position of the individual wires using the track data,
- Faster drift gases (e.g. $Ar/C_2H_6/N_2$),
- The fast increase of the resolution for long drift distances,
- Behaviour in testbeam, preferably in a magnetic field.

The construction of a second P3 chamber is in preparation. The mylar foil with copper strips will be replaced by a plain aluminium foil.

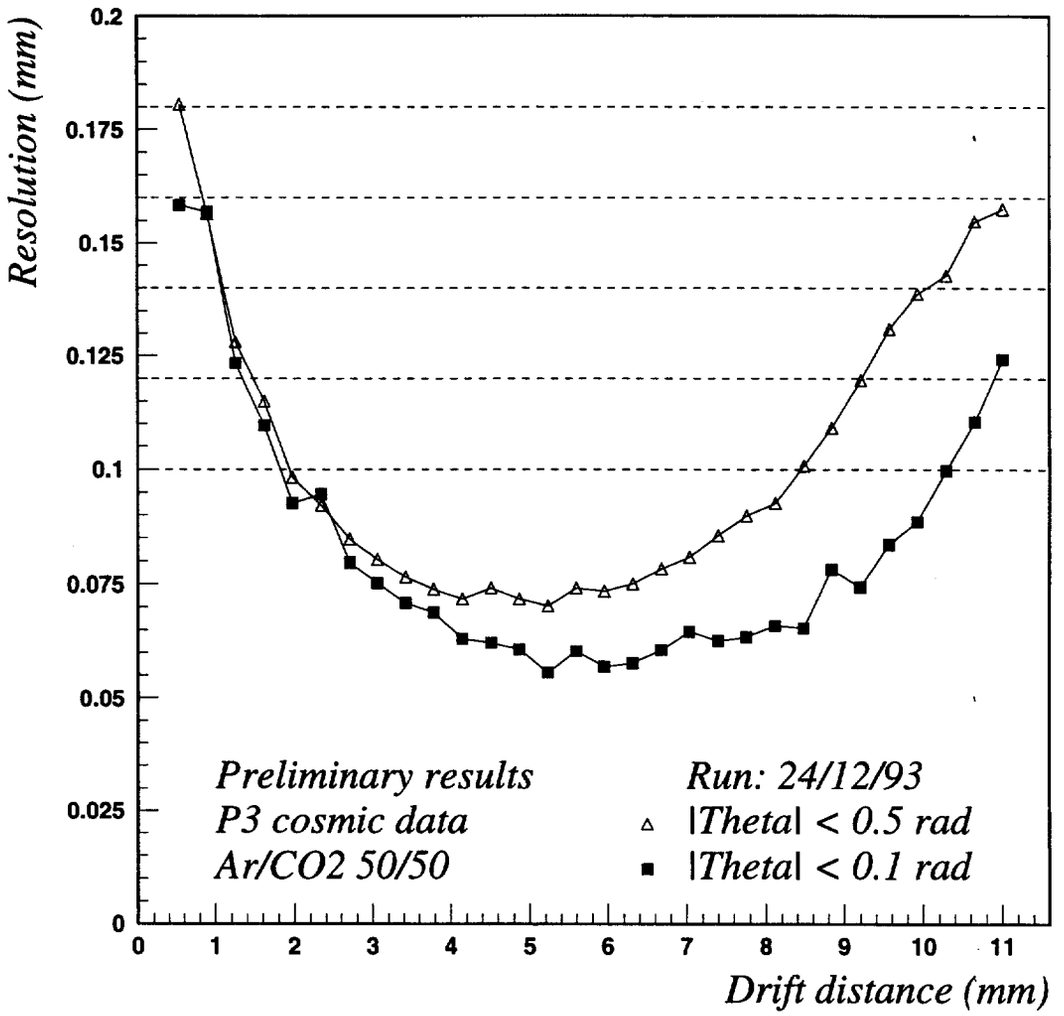

Figure 24: *Spatial resolution vs. the distance to the wire; with a loose and a tight cut on θ.*

4 Muon Spectrometer

4.1 Barrel layout

In the barrel the muon chambers are arranged in three layers: MI, MM and MO. The azimuthal segmentation is shown in figure 25. This layout is dictated by the 8 coils of the air-core toroid. The azimuth region between the coils is covered by "large" chambers; the region occupied by the coils is covered by "small" chambers. Large and small chambers overlap to cover the complete azimuth. The segmentation along the beam direction is shown in figure 26. This segmentation keeps the chamber size manageable, avoids dead zones at chamber boundaries, minimises the number of chamber types and is consistent with the principle of projective alignment to be described in section 5.3.

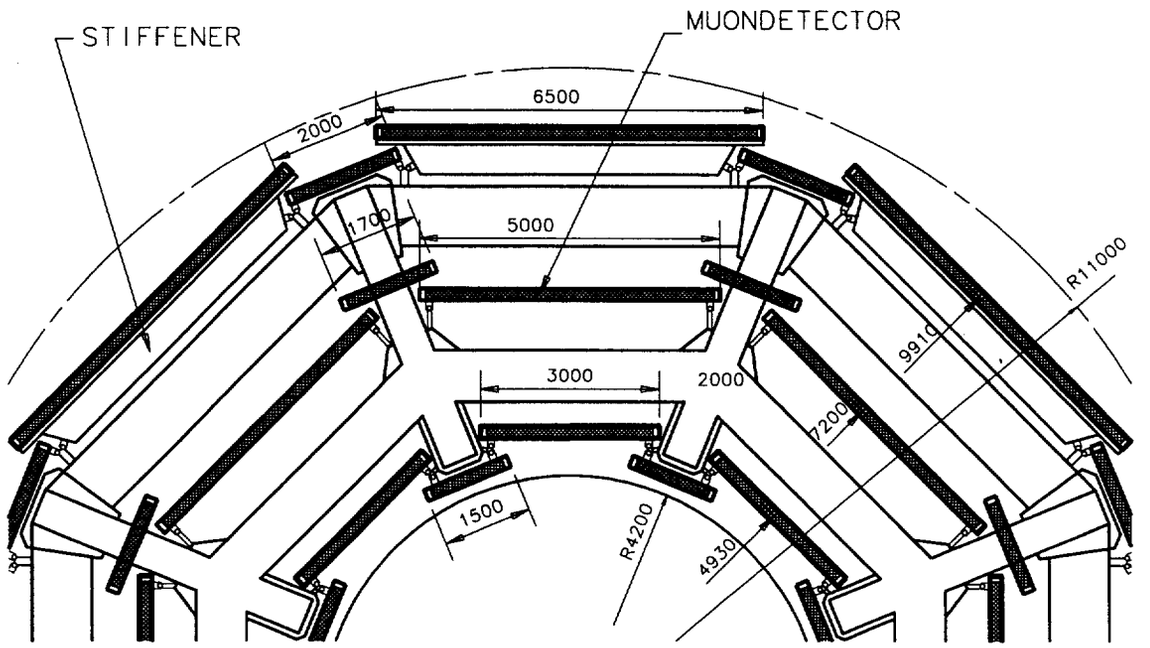

Figure 25: *Barrel muon chambers: azimuthal segmentation.*

The number of chambers of each type and their dimensions are given in tables 3 and 4.

4.2 Endcap layout

No independent engineering studies have been done so far. However, the 2^{nd} coordinate option of the HSC is very attractive for the endcap region, since there the bending will not be perpendicular to the wire direction over the face of a chamber.

In addition the high background levels will probably require a reduced single-cell size. The HSC can go down to a cell diameter of 5 mm.

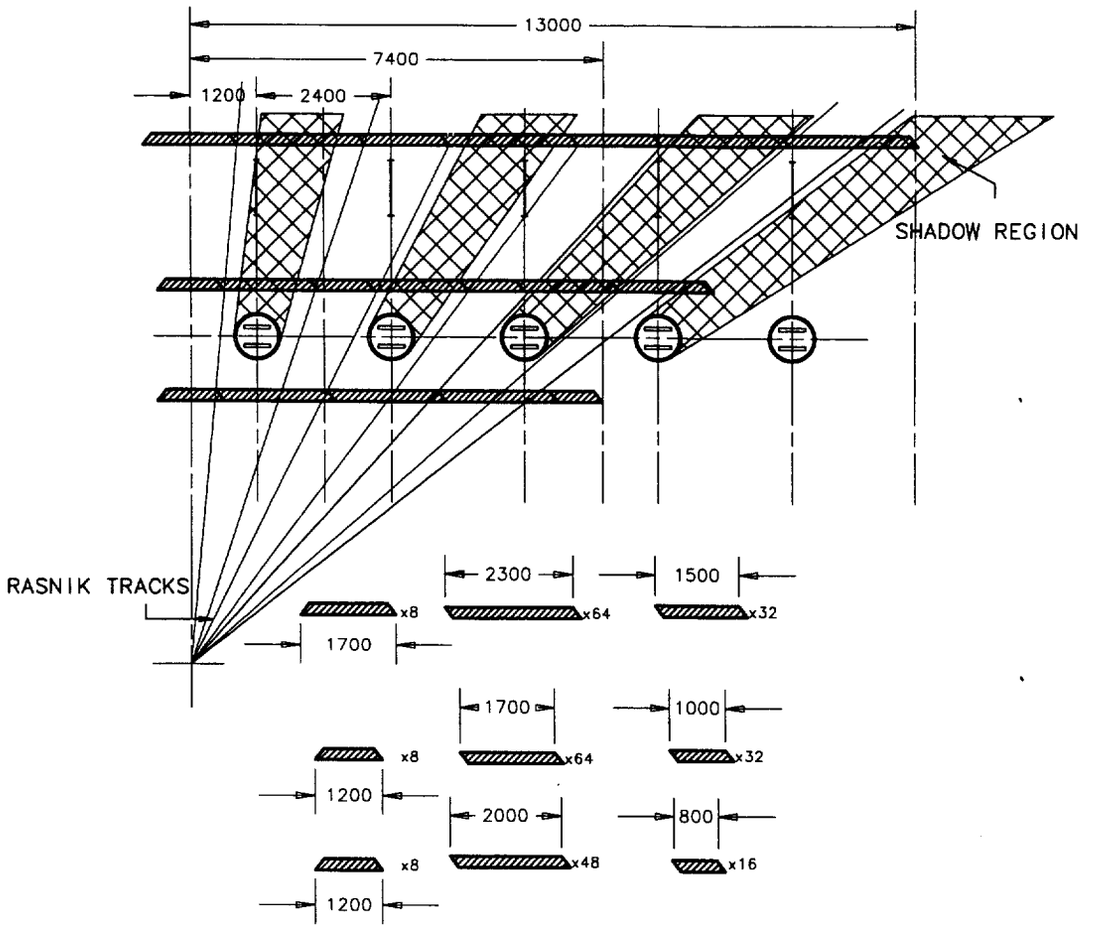

Figure 26: *Barrel muon chambers: longitudinal segmentation.*

4.3 Installation & Support

The chambers are mounted on rails which are fixed at the toroid cryostat vessels. The chamber feet consist of bearings around the rail. The rail is fixed at the cryostat in an early stage. The chambers are lowered into the experimental cavity at the extreme $\pm$ Z sides of the toroid. Here, they are mounted in a 'caroussel' which can move the chambers in X and Y and rotate them to the proper ϕ angle. By moving the chamber in Z, it is shifted onto the rail and put into position and finally adjusted by means of screws.

Almost the complete readout electronic system is mounted on the chamber. Also the HV supplies are integrated with the chamber. The (digital) chamber data are transferred to the counting room by means of optical fibres. The chamber cabling and tubing is, therefore, limited to the optical fibre data lines, low voltage power lines, cables for the alignment systems, gas tubing and, if necessary, cooling tubes. The cabling can be done in an early stage. The chambers can be made operational instantaneously after installation.

Chamber	(Wire)length (mm)	Width (mm)	Thickness (mm)	Number
MI	3000	1200	300	8
	3000	800	300	16
	3000	2000	300	48
MM	5000	1450	560	8
	5000	1000	560	32
	5000	1700	560	64
MO	6500	1700	400	8
	6500	2300	400	64
	6500	1500	400	32

Table 3: *Large (MI, MM and MO) barrel muon chambers.*

Chamber	(Wire)length (mm)	Width (mm)	Thickness (mm)	Number
MI*	1500	2600	–[1]	40
MM*	1700	2000	–[1]	72
MO*	2000	2900	–[1]	72

1: mattress geometry: distance between multilayers to be optimised

Table 4: *Small (MI*, MM* and MO*) barrel muon chambers.*

4.4 Performance

4.4.1 Introduction

In this section we present a short overview of the performance of the HSC option as a muon spectrometer in ATLAS. The basic parameters for this investigation are:

- Wire resolution averaged over a cell: 100 μm ,
- Wire positioning: 25 μm ,
- Station alignment: 30 μm .

The performance of the three options have already been compared in a study by Guyot *et al.* The results have been presented at the ATLAS meeting in November 1993. The general conclusion of this study was that the three options did not show great differences in performance, with respect to muon-resolution as function of momentum and rapidity, background sensitivity, and pattern-recognition. For the HSC results presented here, the main differences as compared to this earlier study are:

- Update of wire resolution, wire positioning and monolayer efficiency,
- More detailed study of the multiple scattering contribution from the chamber and magnet material (struts) in the barrel region.
- Evaluation of the improvement in the momentum resolution when including an angle/angle measurement between the middle and outer stations

4.4.2 Pattern recognition and backgrounds

The consequences of our recent changes (cell-diameter 15 $\rightarrow$ 30 mm, 8 $\rightarrow$ 16 layers in MM) for the pattern recognition or the background sensitivities will be studied in detail. However, we do not expect that the conclusions from Guyot *et al.* will be affected.

4.4.3 Multiple scattering

The general impression presented so far has been that the magnet support material plays such a dominant role over most of the rapidity range that having low-density chambers makes no difference for the momentum resolution. In this section we would like to show :

A) At least 50 % of the spectrometer coverage is free from interference of the magnet material. In this region the multiple scattering from the chambers (MM and the trigger chambers) dominates the momentum resolution in the important momentum range from 30 - 200 GeV.

B) Even in the 'strut-shadow' the multiple scattering from the struts is not so overwhelming that the chamber contributions are negligible, provided we keep this material as far away from the MM chambers as possible.

The chamber contributions to $\Delta p/p$ from multiple scattering are:

- 1.0% from the MM-station material ($0.06 \times X_0$)
- 1.1% from the trigger, assuming that the quoted $0.10 \times X_0$ is distributed in 2 layers separated by +30 cm and -30 cm from the MM mid-plane.

For the magnet strut material we assume :

- an aluminium I-beam of 45 cm height, 30 cm width and 5 cm thickness,
- surrounded by a stainless steel box of 60 cm height, 50 cm width and 1 cm thickness.

By default the struts are positioned halfway between the MI and MM stations. The resulting $\Delta p/p$ contribution as a function of η is shown in figure 27 for 5000 muons of 100 GeV. Averaged over the barrel and away from the coils proper the contribution to $\Delta p/p$ is 1.4%. This value shifts to 2.0% (1.1%) if the strut is positioned 50 cm closer to (further away from) the MM station. For muons going through a strut halfway between MI and MM the average multiple scattering contributes about 3.0% to $\Delta p/p$.

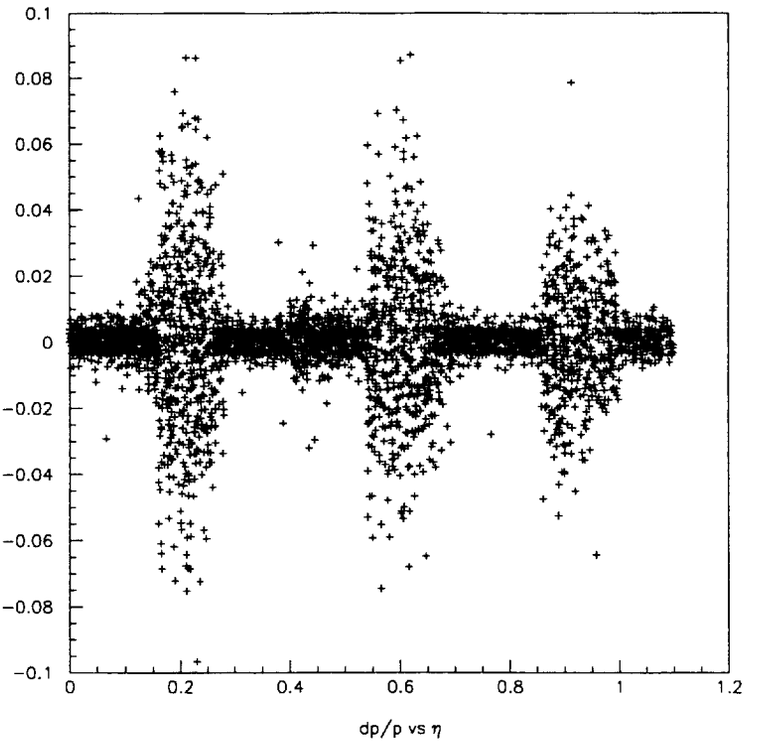

Figure 27: *The $\Delta p/p$ contribution from the magnet struts only, as a function of pseudorapidity for 100 GeV muons measured in the barrel spectrometer. In this plot the scattering in the region between the struts is due to air (+ some localised scatterings from the upper I-beams between MM and MO). In azimuth the muons go through the middle of an octant.*

4.4.4 Momentum resolution

In figure 28, the different contributions to the transverse momentum resolution $\Delta p_T / p_T$ are plotted as a function of pseudorapidity η for $p_T = 100\ GeV$, in the barrel region and in between the coils. The multiple scattering contribution is shown separately for the struts and for the MM+trigger material. In the barrel region ($\eta < 1.1$) the former dominates for about $\frac{1}{3}$ of the the rapidity coverage, while the latter dominates for the rest.

The contributions are compared as a function of momentum in figure 30. Here, the lines show the 'incremental' effects on the resolution, starting with the intrinsic resolution of the HSC spectrometer. In order to facilitate the comparison with the other spectrometer options a sagitta error of 50 μm has been used. This would correspond to a (pessimistic) HSC single wire resolution of 135 μm in the present layout (see table 1). The other lines are calculated by successively adding the contributions from the alignment, the multiple scattering, and the energy-loss correction. For the uncertainty in the energy-loss correction we used the same formula as used by Guyot in earlier comparisons : $\Delta p/p = 0.5 + 26/p(GeV)$ %. The dominant contribution in the important momentum regions between 30 and 200 GeV for the strut-free case, and between 30 and 500 GeV for the strut-shadow case, comes from multiple scattering.

It is therefore certainly advantageous to keep the chamber and trigger material of low density and the struts as far away from the middle layer as possible.

We now estimate the gain in resolution that can be obtained by combining the sagitta measurement with an angle/angle measurement of the muon momentum using the track segments in the MM and MO stations. Above 20 GeV this measurement is not dominated by multiple scattering and almost uncorrelated with the sagitta measurement. For this estimate we use a 'matras' layout of the MM and MO stations with a 20 cm stiffener between the 2x8 and 2x4 monolayers respectively. This provides an angle/angle measurement of the momentum with a resolution of :

$$\Delta p/p = \sqrt{2^2 + (0.092 * p(GeV))^2}\ \%$$

which can be combined with the sagitta measurement, taking into account the common uncertainty in the energy-loss correction. For momenta below 100 GeV an appreciable gain is obtained in the strut-shadow region. As an example the result of this procedure is plotted in figure 29 as function of pseudorapidity for a transverse momentum of 50 GeV.

Finally, in order to show the effect of an improvement in the HSC single wire resolution, we plot in figure 31 the $\Delta p/p$ band corresponding to average single wire resolutions between 80 and 100 μm .

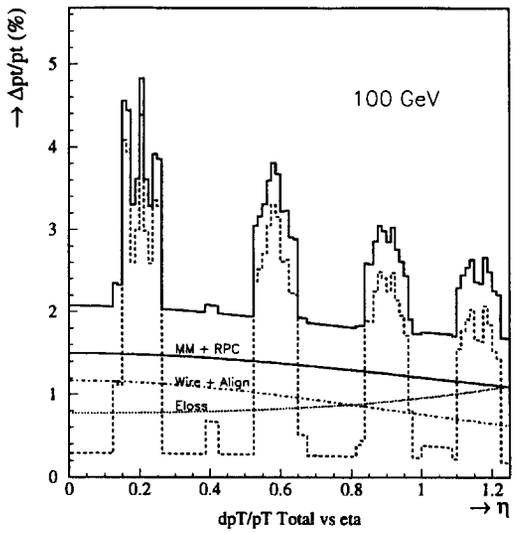

Figure 28: *Summary of the $\Delta p_T / p_T$ contributions as a function of pseudorapidity for $p_T = 100$ GeV.*

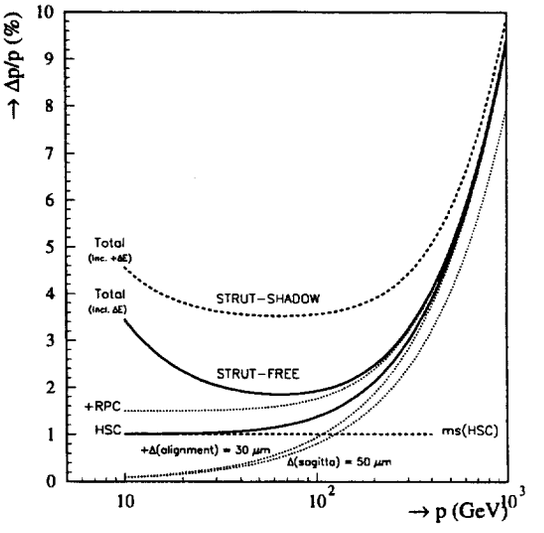

Figure 30: *Summary of the $\Delta p/p$ contributions as function of muon momentum.*

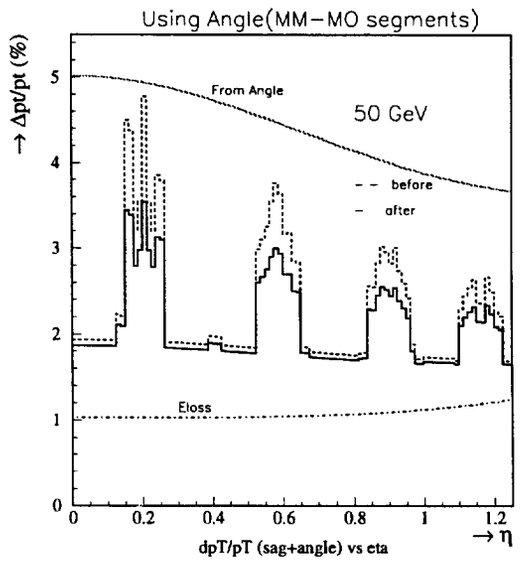

Figure 29: *Effect of combining sagitta and angle/angle momentum measurements on $\Delta p_T / p_T$ as function of pseudorapidity for $p_T = 50$ GeV.*

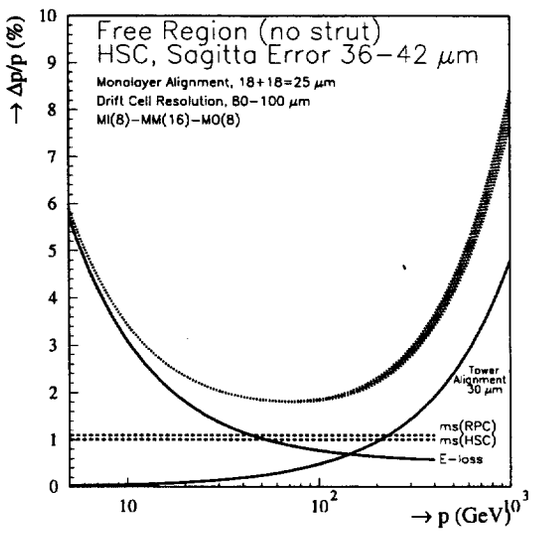

Figure 31: *$\Delta p/p$ as function of muon momentum, for average single-wire resolutions in the range 80 - 100 μm .*